Published in *Engineering Structures* 191 **2019** pp. 1-11

Drive-by scour monitoring of railway bridges using a wavelet-based approach

Paul C. Fitzgerald[a,1*], Abdollah Malekjafarian[a,2], Daniel Cantero[b,3], Eugene J. OBrien[a,4], Luke J. Prendergast[c,5]

*Corresponding author.

[a] School of Civil Engineering, University College Dublin, Dublin, Ireland

[b] Department of Structural Engineering, Norwegian University of Science and Technology (NTNU), Trondheim, Norway

[c] Department of Civil Engineering, Faculty of Engineering, University of Nottingham, Nottingham, NG7 2RD, United Kingdom.

E-mail: [1]paul.fitzgerald.3@ucdconnect.ie, [2]abdollah.malekjafarian@ucd.ie, [3]daniel.cantero@ntnu.no, [4]eugene.obrien@ucd.ie, [5]luke.prendergast@nottingham.ac.uk

Abstract

This paper numerically investigates the feasibility of using bogie acceleration measurements from a passing train to detect the presence of bridge scour. The Continuous Wavelet Transform is used to process the simulated acceleration measurements for a number of train passages over a scoured bridge, with scour represented as a local reduction in stiffness at a given pier. Average Wavelet coefficients are calculated for a batch of train runs passing over the same bridge. A scour indicator is developed as the difference in average coefficients between batches from the healthy bridge and when the bridge is damaged by scour. The method is assessed using a blind test, whereby one author simulated trains passing over a bridge in various states of health. The remaining authors were provided only with the train accelerations and had to predict the state of scour without any prior knowledge. This scour indicator performed quite well in the blind test for normal vehicle operating conditions.

1. Introduction

Scour is the term used to describe the excavation of soil from around foundations due to adverse hydraulic actions [1] and is a primary cause of bridge failure worldwide [2, 3]. Scour occurs in different forms: general scour occurs due to natural river bed evolution [4, 5]; contraction scour occurs due to increased water velocities at the location of bridge openings [6]; and local scour occurs due to the presence of obstacles such as bridge sub-structure elements obstructing the flow [1]. These combined scour cases can have a deleterious effect on bridge performance [7] and can lead to sudden failure.

In piled bridges, scour leads to an increase in the unsupported height of piles, which can cause failure due to pile buckling [8] and reduces the bridge lateral stiffness. For bridges comprised of simply-supported spans and founded on shallow foundations, scour can undermine the foundation, reducing the contact area between the foundation and the underlying soil. In addition to the reduction in effective stress at formation level due to the soil removal, the reduced contact area leads to increased stress on the remaining soil. Increased stress leads to increased strain, which ultimately leads to reduced foundation stiffness due to the nonlinear strain-dependency of soil stiffness [9]. For bridges comprised of continuous spans founded on shallow foundations, it should be noted that under scour, some stress redistribution will occur throughout the bridge, which will mitigate the stiffness reduction under scour.

Recognising that scour ultimately leads to reductions in stiffness has encouraged researchers to apply vibration-based damage detection approaches to detect and monitor the presence of scour erosion [10-12]. Works to date have mainly focussed on methods that require the installation of vibration sensors on the bridge to monitor changes in modal properties (frequencies and mode shapes). Klinga and Alipour [13] numerically investigate the performance of various bridge elements (piles, abutments) under extreme scour, and conclude that the bridge's frequency and lateral stiffness reduce under scour. Ju [14] investigates how the natural frequency of a bridge varies with scour, accounting for the effects of water-added mass, and concludes that the bridge frequency is lower in the presence of water than in its absence. Prendergast et al. [15, 16] numerically investigate the feasibility of detecting and locating scour damage using the lateral vibrations of a two-span integral bridge traversed by a vehicle. The influence of vehicle-bridge interaction parameters such as speed, mass, and axle stiffness are studied. They conclude that detecting scour using vibrations arising in the structure due to a passing vehicle is promising. Several authors have performed full-scale field testing to detect scour using vibration-based approaches. Foti and Sabia [17] carried out a study on a five-span bridge where one of the piers was adversely affected by scour. The pier was monitored to ascertain if it were possible to detect asymmetric dynamic behaviour due to uneven scour affecting the pier. Using the covariance of accelerations, they conclude that scour presence was detectable but quantifying its extent was not. Chen et al. [18] implement a vibration-based scour approach using ambient velocity measurements on a cable-stayed bridge. By combining the measurements with finite-element updating, they successfully quantify scour at the pier. Xiong et al. [19] also apply a vibration-based approach to a cable-stayed bridge, and investigate the application of four dynamic indicators, namely frequency change ratio, modal assurance criterion, mode shape curvature, and flexibility-based deflection. They recommend the flexibility-based deflection approach as a sensitive and practical scour indicator.

The above research into vibration-based scour monitoring methods may be predominantly classified as *direct methods*, as they use information from sensors physically installed on the bridge. *Indirect monitoring*, or 'drive-by' methods, use responses from sensors installed on a passing vehicle to infer information on the bridge condition. The vehicle is used to both excite and measure the bridge response. Drive-by approaches can be advantageous in that a moving sensor (vehicle) passes over every point along the length of the bridge as opposed to a fixed sensor, which is stationary. This leads to improved spatial information, which can be desirable for damage detection [20]. The application of drive-by approaches to scour has, to the best of the authors' knowledge, not been considered previously. However, these approaches have been applied to detect other types of damage, and a brief review of these works is presented here. For a more extensive review, see Refs. [21-24].

Generally, indirect approaches aim to extract dynamic properties of a bridge, such as frequencies or mode shapes. Changes in these parameters can then be used to infer the presence of structural damage. Extracting bridge frequencies from a vehicle response was first theorised by Yang et al. [25]. Subsequent experimental verifications to extract the bridge fundamental frequency from the vehicle response have been carried out by Lin and Yang [26], who suggest that a heavier vehicle can aid the extraction of the bridge frequency due to the increased amplitude of the bridge response. Multiple vehicle crossings also improve the approach. Oshima et al. [27] confirms the value of a heavier vehicle, and uses an excitation machine in addition to the vehicle in an effort to obtain a more consistent bridge response. Malekjafarian et al. [21] note the optimal conditions required for bridge frequency extraction. These include (i) low vehicle speeds (below 40 km/h), (ii) multiple vehicle crossings (at least three), and (iii) the use of a heavy vehicle and/or an exciter to increase bridge excitation. Other authors have shown that it is possible to extract bridge mode shapes from a vehicle response. Mode shape estimations are useful in that scour damage is often localised, and mode shapes are sensitive to local changes in the structure [28, 29].

Additionally, there are also drive-by methods that do not explicitly use the estimation of bridge dynamic properties as a means of monitoring its condition. OBrien et al. [30] propose a Moving Force Identification (MFI) algorithm to monitor highway infrastructure using vehicle accelerations. Road surface profile and global bridge stiffness are then obtained from the calculated vehicle-bridge interaction force. The approach is verified in an experimental investigation [31]. A significant drawback of the approach is that the dynamic properties of the vehicle (suspension stiffness, damping etc.) need to be known.

Several authors have used wavelet transforms in drive-by applications. The wavelet transform allows for a time-frequency representation of a signal, which is useful for locating damage. While the Short Time Fourier Transform (STFT) also provides time-frequency information, wavelet analysis offers greatly improved resolution capabilities. This is because the window size in STFTs is fixed for all frequencies. Increasing the window size improves the frequency resolution, but at the expense of losing time information [32]. Wavelet analysis solves this by allowing for a variable window size, meaning that good time resolution can be obtained for long signals, and good frequency resolution can be obtained for high frequency signals [33]. McGetrick and Kim [34] use the Continuous Wavelet Transform (CWT) with the Morlet wavelet to analyse the acceleration response of a vehicle crossing a bridge. A damage indicator based on the CWT coefficients is found to be capable of distinguishing between different levels of crack severity on a bridge. Hester and González [22] have numerically shown that bridge cracks can be detected using the CWT of vehicle accelerations with the Mexican Hat wavelet. Khorram et al. [35] numerically compare the results of applying the CWT to simulated measurements from a bridge, and then a crossing vehicle. It is found that the moving sensor approach (i.e. the vehicle response) is more effective than the fixed sensor approach (on the bridge) at detecting small cracks.

In this work, a drive-by approach is postulated to detect scour using modelled accelerations measured on a train bogie. The CWT using the Complex Morlet wavelet is applied to the bogie accelerations generated for multiple train passages over a bridge and the moduli of the wavelet coefficients are then interpolated to vehicle position on the bridge (in lieu of time). This allows the moduli to be averaged over multiple vehicle crossings. A scour indicator is defined as the difference in the average moduli between batches of crossings from healthy and scoured bridges. Section 2 presents details of the numerical modelling of the train-bridge system used to demonstrate and test the approach. Section 3 introduces the wavelet-based scour detection approach. Section 4 presents the implementation of the approach and studies various vehicle-bridge interaction effects on the robustness of the method. Finally, Section 5 presents the assessment of the approach through a more detailed numerical case study and a blind test, where the team seeking to identify scour do not know the results in advance.

2. Numerical Modelling

Fig. 1 shows a schematic of the finite-element numerical model used to introduce and test the approach in this paper (a more advanced model is used in Section 5 of the paper). The numerical modelling and post-processing was undertaken in the MATLAB programming environment.

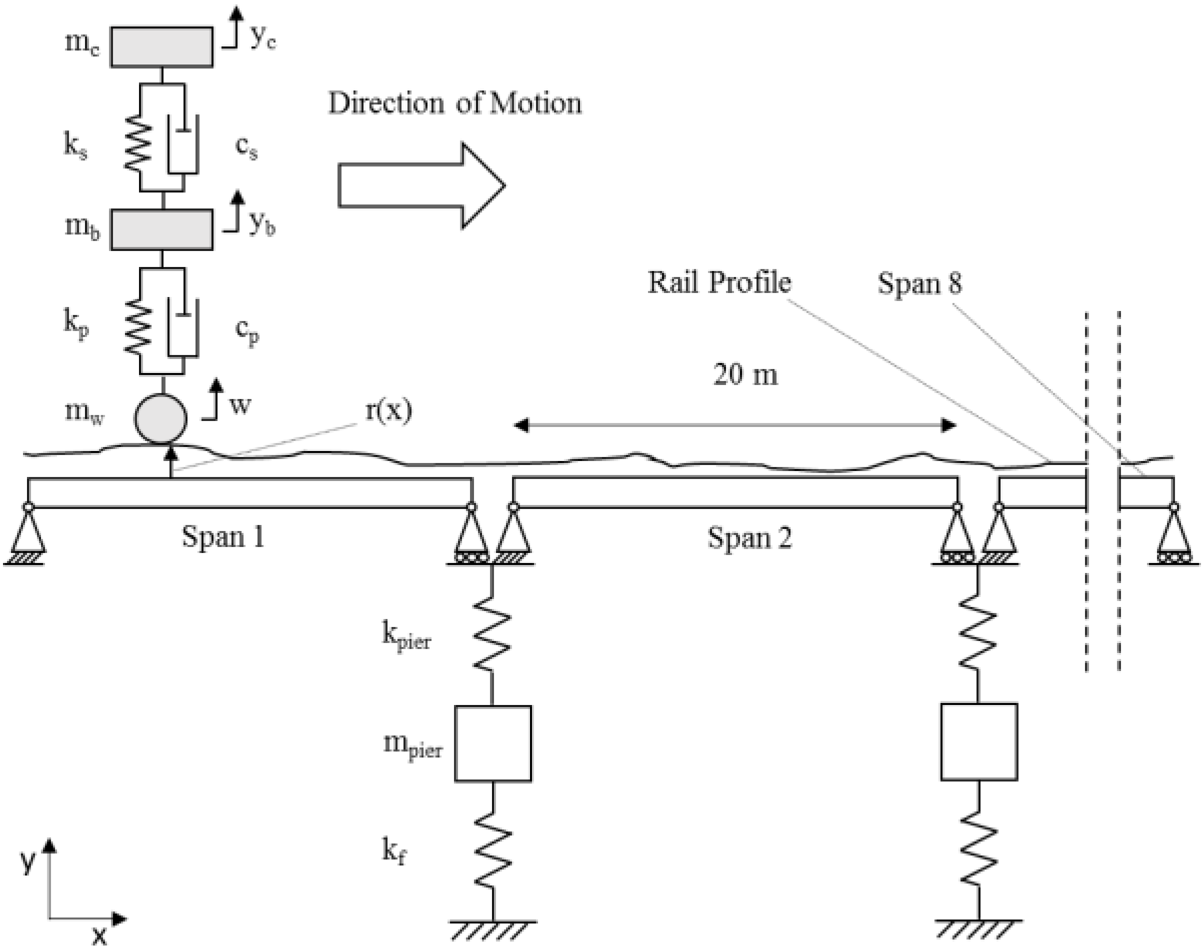

Fig. 1: Schematic of complete system

The model in Fig.1 primarily consists of two dynamic sub-systems, namely the vehicle and the bridge, which interact. The bridge model comprises multiple spans with pinned connections over the piers. Each pier is assumed to be founded on a shallow pad foundation with underlying soil stiffness. The bridge surface contains a rail profile to simulate surface unevenness. The train model is a simplified two-degree-of-freedom (2-DOF) model of half a train carriage. A mass representing a train wheel is assumed to remain in contact with the rail profile on which it is travelling. In modelling terms, it is assumed to be part of the bridge system and its vertical position, w, is simply the sum of the profile plus the bridge deflection directly underneath it.

2.1 Train model

The train model consists of a 2-DOF quarter-car model, deemed to represent one bogie and half of the body mass of the train carriage. From Fig. 1, the bogie mass, half the carriage mass, the primary suspension stiffness and damping, and secondary suspension stiffness and damping, are represented by m_b, m_c, k_p, c_p, k_s and c_s respectively. The mass of the train wheels for half a train carriage are represented by m_w. By maintaining constant contact between wheel and profile, the vertical position of the wheel at any moment in time may be described by:

$$w = r + b \tag{1}$$

where r represents the rail profile between the wheel and the bridge and b is the vertical deflection of the bridge underneath. The dynamic system may be represented by Eq. (2).

$$[M_A]\{\ddot{y}\} + [C_A]\{\dot{y}\} + [K_A]\{y\} = \{f_A\} \tag{2}$$

where M_A, C_A, K_A are the vehicle mass, damping and stiffness matrices respectively and y is a vector of vehicle displacements:

$$\{y\} = \begin{Bmatrix} y_c \\ y_b \end{Bmatrix} \tag{3}$$

where y_c and y_b denote the displacements of the body and bogie degree of freedoms respectively. f_A is an external force vector as shown in Eq. (4):

$$\{f_A\} = \begin{Bmatrix} 0 \\ k_p w + c_p \dot{w} \end{Bmatrix} \tag{4}$$

where $\dot{w}$ denotes the first derivative of w with respect to time. The parameters of the quarter-car model in this study are listed in Table 1. They are based on a paper by OBrien et al. [36], who calibrate a full train carriage model using acceleration responses from an in-service train.

Table 1: Vehicle parameters used in study

Property	**Symbol**	**Unit**	**Value**
Carriage mass	m_c	kg	18.4×10^3
Bogie mass	m_b	kg	3.9×10^3
Wheel mass	m_w	kg	2.8×10^3
Primary suspension stiffness	k_p	kN/m	5.6×10^3
Secondary suspension stiffness	k_s	kN/m	1×10^3
Primary suspension damping	c_p	kN s/m	58.8
Secondary suspension damping	c_s	kN s/m	60

2.2 Bridge model and coupled train-bridge interaction

The bridge consists of eight 20 m spans, each modelled as a simply supported Euler-Bernoulli beam [28], with depth and second moment of area of 1 m and 0.33 m^4 respectively. The second moment of area is calculated assuming a 4 m wide single-track railway bridge with a rectangular cross-section. Each beam has modulus of elasticity and mass per unit length of 35×10^6 kN m^{-2} and 9.6×10^3 kg m^{-1} respectively. Each Euler-Bernoulli beam is modelled using twenty 1 m long elements. The beam connections are modelled as nodal (internal) hinges and the bridge external boundaries are assumed to be on undeformable abutments with pinned and roller supports. The bridge contains seven piers, each is modelled with a single DOF in the vertical direction. The mass (m_{pier}) and stiffness (k_{pier}) of each pier is 42 tonnes and 12.5×10^6 kN/m, respectively. These values are calculated by assuming a pier 7 m high (in *y*-direction), 1 m long (in *x*-direction) and 2.5 m wide (into the page) with modulus of elasticity and density of 35×10^6 kN m^{-2} and 2400 kg m^{-3} respectively. Underneath each pier is a spring, k_f, representing the vertical stiffness provided by a shallow pad foundation 4 m long (into the page) and 2 m wide (*x*-direction). By assuming that the bridge is founded on a rigid footing overlying a soil profile corresponding to medium dense sand with Young's modulus, E=100MPa [37] the spring stiffness, k_f, is found to be 344×10^3 kN/m, using the approach in [38].

The bridge dynamic response is modelled using Eq. (5).

$$[M_B]\{\ddot{u}\}+[C_B]\{\dot{u}\}+[K_B]\{u\}=[L]\{f_b\} \tag{5}$$

where M_B, C_B and K_B are the system mass, damping and stiffness matrices respectively, and u, $\dot{u}$ and $\ddot{u}$ are the displacement, velocity and acceleration respectively. Damping is incorporated in the bridge system using a Rayleigh damping approach and 3% damping is assumed [29]. The mass of the train wheels are coupled with the bridge system so the mass matrix, M_B, is time-varying as the vehicle moves across the bridge. The vector f_B contains the interaction forces applied to the bridge by the vehicle, and is time-varying. These forces are distributed to the relevant degrees of freedom using a location matrix L, which takes into account the position of the vehicle at each time-step. Both the vehicle and the bridge influence one another (i.e. they are coupled), and the coupled system may be represented by:

$$\begin{bmatrix} M_A & 0 \\ 0 & M_B \end{bmatrix} \begin{Bmatrix} \ddot{y} \\ \ddot{u} \end{Bmatrix} + \begin{bmatrix} C_A & C_{A,B} \\ C_{B,A} & C_B \end{bmatrix} \begin{Bmatrix} \dot{y} \\ \dot{u} \end{Bmatrix} + \begin{bmatrix} K_A & K_{A,B} \\ K_{B,A} & K_B \end{bmatrix} \begin{Bmatrix} y \\ u \end{Bmatrix} = \{ F_g \} \tag{6}$$

where F_g represents the coupled system force vector. The profile present on the bridge is shown in Fig. 2. It is an FRA Class 4 rail profile that is randomly generated using Power Spectral Density functions [39]. Entry and exit distances are assumed as 50 m both before and after the bridge, making the total length of profile 260 m. The entry/approach length is used to negate transient vehicle effects when the vehicle arrives on the bridge. The exit length is simply used to ensure that there is enough signal to remove any edge effects when applying the wavelet method later.

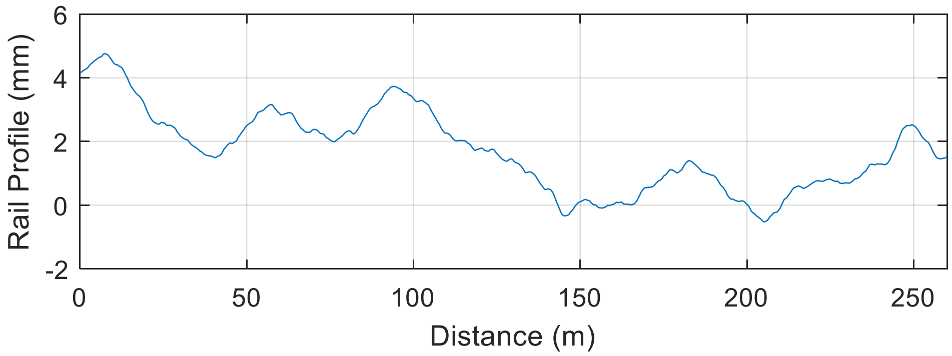

Fig. 2: Rail profile

2.3 Scour modelling

Scour is modelled in this paper as a reduction in vertical foundation stiffness k_f (Fig. 1). Due to the potential for scour to undermine shallow foundations, reducing the contact area between the foundation and underlying soil, coupled with the strain-dependence of soil stiffness, a reduced soil-foundation contact area can result in relatively large reductions in stiffness. In this paper, a maximum (extreme) stiffness loss of 30% is assumed, which corresponds to scour undermining the foundation and reducing the soil-foundation contact area from $8m^2$ to approximately $5m^2$, with a corresponding reduction in soil shear modulus of 10% [40]. The global mode shapes of the bridge can be extracted by solving the Eigenproblem [29]. Table 2 shows the first ten frequencies of the bridge system. Fig. 3 shows the change in the first global mode shape of the bridge as a result of reducing the value of k_f at the 60 m position by 30%. It is clear that there is a significant change in the mode shape as a result, and this change should also affect the vehicle response. By examining Eqs. (2-4), it can be deduced that the vehicle model is excited with a term containing the deflection of the bridge.

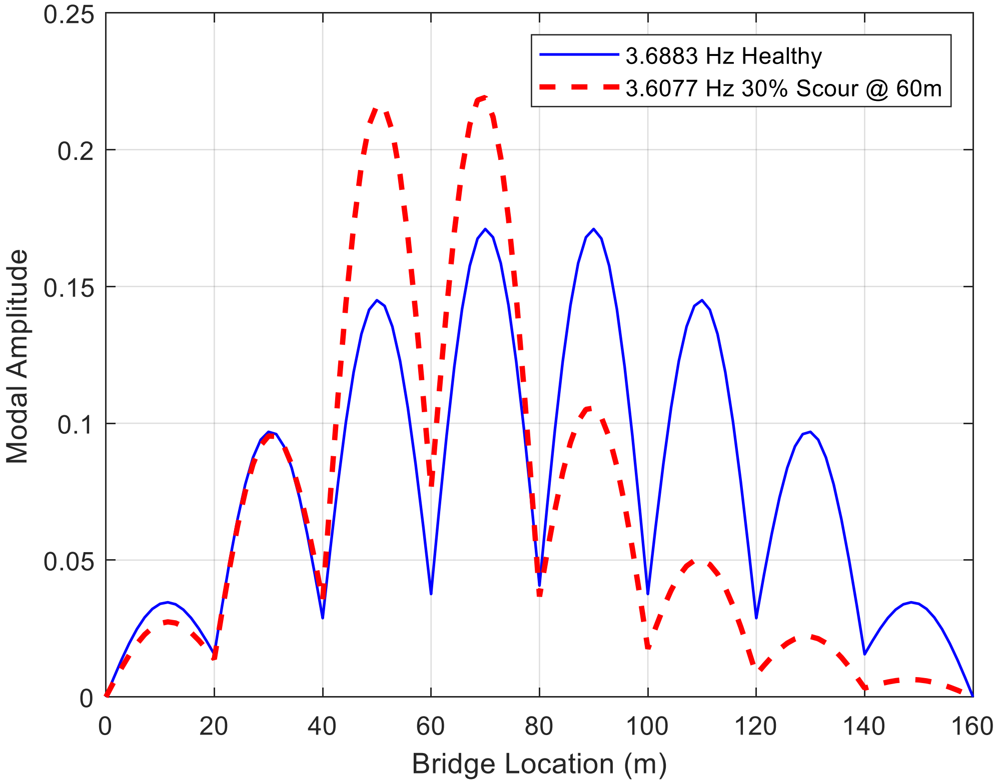

Fig. 3: Change in first mode shape of bridge due to scour at 60 m point

Table 2: Bridge modal frequencies

Mode Number	**Frequency**		**Mode Number**	**Frequency**
1	3.69 Hz		6	4.20 Hz
2	3.74 Hz		7	4.29 Hz
3	3.83 Hz		8	4.33 Hz
4	3.94 Hz		9	8.64 Hz
5	4.07 Hz		10	8.96 Hz

2.4 Addition of noise to bogie accelerations

The acceleration signals generated in the numerical model are clean, in the sense that they do not contain any random variations that real accelerometer readings would. Sensor noise is the presence of random oscillations in accelerometer readings, and these determine the minimum resolution of a sensor. To make the readings more realistic in this paper, random noise is added to the acceleration signals using Eq. (7):

$$\{a\} = \{a_{calc}\} + E_p \{N_{noise}\} \sigma \tag{7}$$

where a is the polluted acceleration signal, E_p is the level of noise, N_{noise} is a normally distributed vector with a unit standard deviation, a_{calc} is the clean acceleration signal outputted from the vehicle-bridge interaction model and σ is its standard deviation. The level of noise in accelerometer readings is a function of the type of quality of the sensors, and the technology used to record the data. Noise level is arbitrarily chosen to be 5% for this study, which is consistent with values used in the literature [41-45]. It should be noted that there are other sources of noise in vehicle-based accelerometer readings, which manifest as frequencies in response spectra resulting from variations in vehicle behaviour such as speed. By varying the mass and speed of vehicles used in this study, these influences are also incorporated. It is recommended that experimental verification be carried out to ascertain the magnitude of noise expected from sensors placed on train bogies.

3. Scour Detection Technique

3.1 Wavelet choice

The damage indicator proposed in this paper is based on the Continuous Wavelet Transform (CWT), explained in detail in [45]. The Morlet Wavelet, adopted in previous SHM applications [46], is used in the current study. The Morlet Wavelet can be defined as in Eq. (8)

$$\psi(x) = \frac{1}{\sqrt{\pi F_b}} e^{j2\pi F_c x - x^2/F_b} \tag{8}$$

where F_b is known as the bandwidth parameter, which is defined as the variance of the Fourier transform of the wavelet, and F_c is the centre frequency of the wavelet [47]. The Morlet is a Complex valued wavelet but often only a Real valued Morlet wavelet is used in SHM applications. A Real Morlet wavelet may be obtained by simply using the Real part of the Morlet wavelet defined in Eq. (8). By selecting appropriate values of F_b and F_c in Eq. (8), a

Morlet wavelet can be created. In this study, a Morlet wavelet with values of F_b and F_c equal to 1 and 1.5 respectively is used [47].

While Real wavelets are commonly adopted for SHM applications [48], a wavelet comprising of only a Real part (i.e. non-Complex valued) is not suitable for the application in this paper. Acceleration signals are being used to detect scour, which have both amplitude and phase. As a result, applying the CWT to an acceleration signal will result in coefficients that oscillate between positive and negative values. This is due to the fact that the analysing wavelets are changing from between being in phase and out of phase with the portion of the signal being analysed in the CWT process.

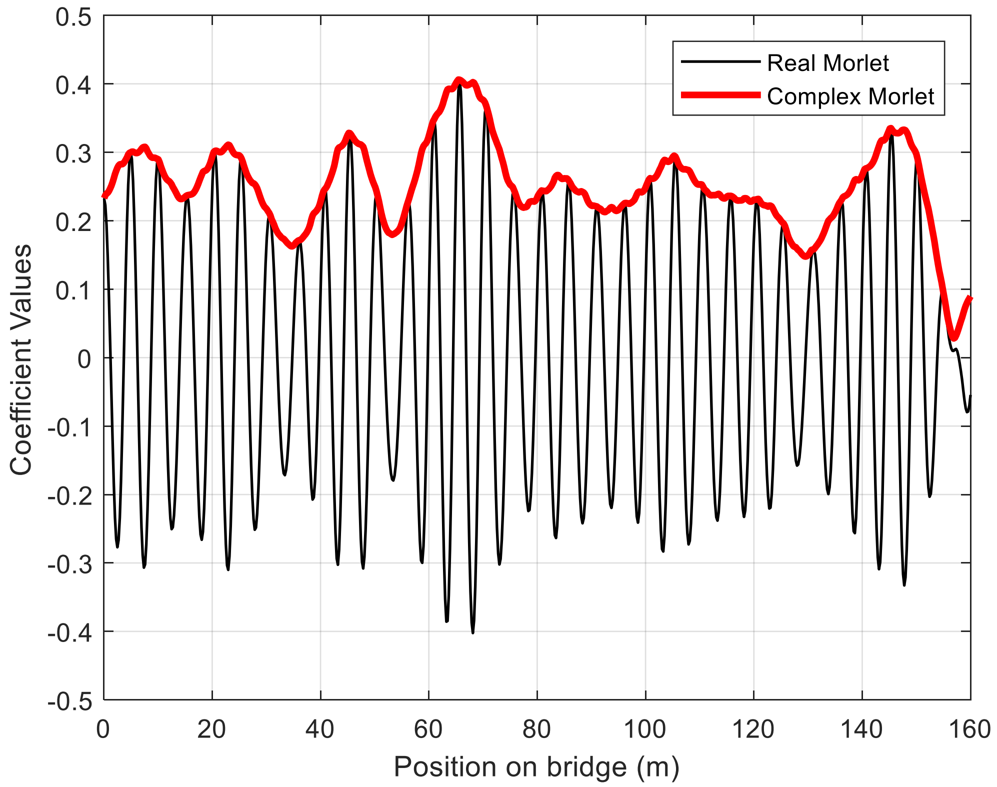

Fig. 4: Real Morlet coefficients vs Complex Morlet coefficients (moduli) for scale corresponding to an arbitrarily chosen equivalent frequency of 4.8 Hz.

Fig. 4 shows an example of the coefficients obtained using a Real Morlet wavelet and the Complex one for bogie accelerations due to a vehicle crossing at 80 km/h. An arbitrarily chosen scale is depicted in the figure, and the coefficients are plotted against vehicle position on the bridge. The acceleration signal to which the CWT is applied is a healthy (unscoured) acceleration signal – see Fig. 5. In this work, the phase issue incurred by applying the CWT to the acceleration signal is addressed by using the Complex Morlet wavelet and taking the moduli of the coefficients (Fig. 5).

3.2 Scour detection using wavelet coefficient differences

In this section, wavelet coefficient differences are proposed to detect scour. The quarter-car (train model) with properties described in Table 1, is simulated crossing the bridge at 80 km/h for healthy and scoured cases. In this example, scour is represented as a loss in stiffness, k_f, of 30% at the 60 m point on the bridge. Fig. 5 shows the acceleration of the bogie DOF for the pre-scour and post-scour cases. The acceleration is plotted against vehicle position on the bridge (instead of time). It can be seen that there are differences between the signals before and after the scoured location (60 m point), and the biggest differences are seen around the location of the scoured pier.

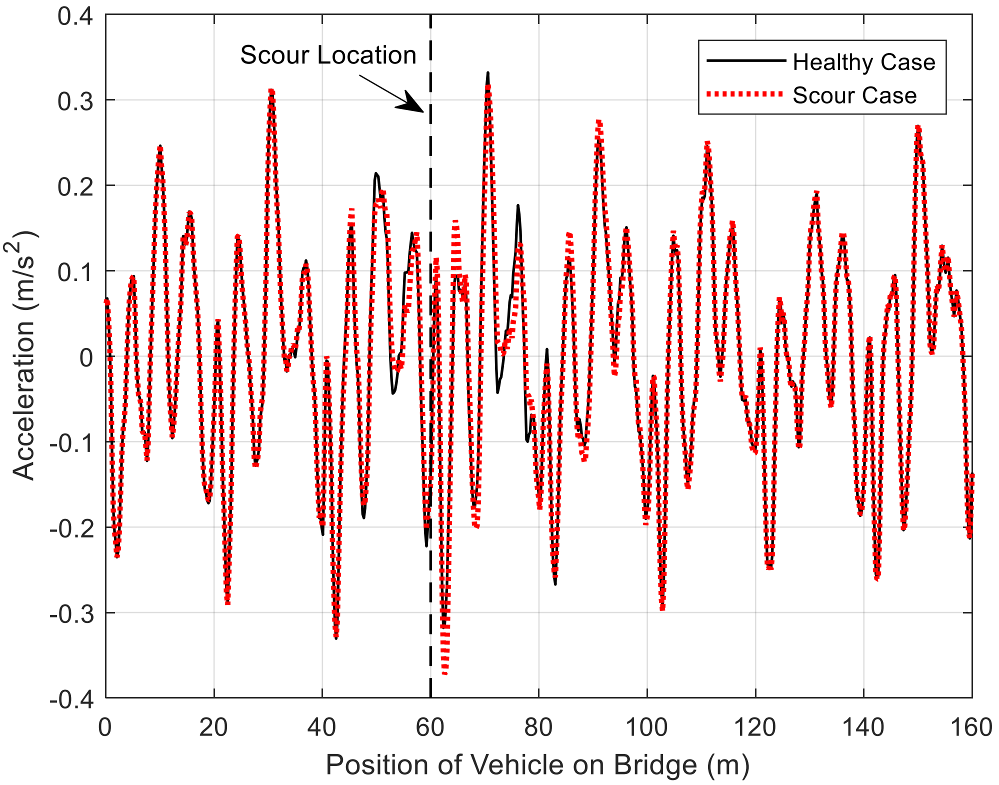

Fig. 5: Effect of scour on bogie acceleration

Simply applying the CWT to the acceleration signal for the scoured case, there are no obvious peculiarities in the coefficients. This is unsurprising as the differences in the accelerations shown in Fig. 5 are small relative to the signal amplitude. However, by first applying the CWT to the healthy signal, and then to the scoured signal, it is possible to detect scour by subtracting the healthy and scoured coefficients.

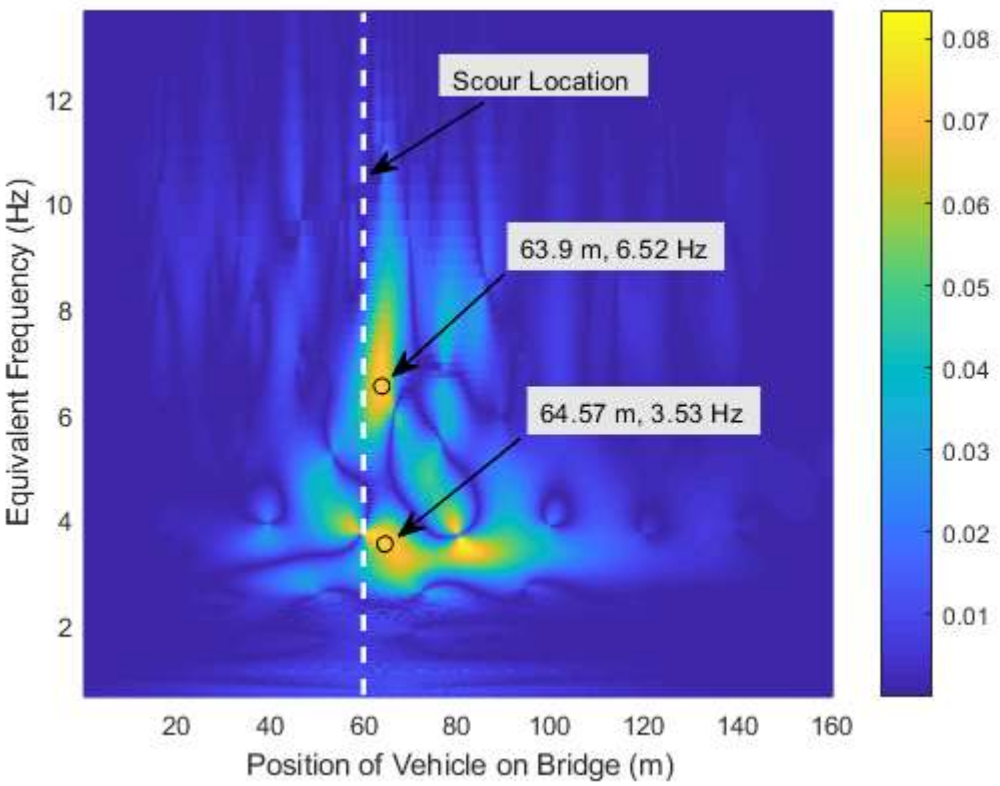

Fig. 6 Absolute value of differences between healthy and scoured wavelet coefficients (i.e. modulus of coefficients) minus scoured acceleration coefficients using Complex Morlet wavelet

Fig. 6 shows the results of subtracting the moduli of the coefficients of the signals shown in Fig. 5 and taking the absolute values of the differences. There are two frequency regions, which have large values (shown as tending towards yellow in the colour plot). The first region is in the range of 3-4 Hz in Fig. 6, and the second region is in the range of 6-8 Hz. The region between 3-4 Hz relates to the change in the modes of vibration of the bridge model due to scour. Table 2 shows the frequencies of the first 10 modes of the healthy bridge system. The first mode shape of the system is shown in Fig. 3. It has a frequency of 3.69 Hz (for the healthy case) and it reduces significantly to 3.61 Hz due to the presence of scour at one pier. The second region in Fig. 6 (between 6-8 Hz) relates to the change in excitation of the bogie (which has a frequency of 6.55 Hz) due to the influence of the changed ‘apparent profile’ as a result of scour. The apparent profile is the excitation experienced by the vehicle and is simply the sum of the profile (between bridge and rail) plus the bridge deflection beneath the vehicle [49]. This change may also be understood by examination of Eqs. (2-4). It should be noted that within the bridge frequency range, a bright spot is observed to extend from the 60m point to the 80m point. The reason for this is the difference in excitation provided to the vehicle by the scoured structure relative to the unscoured structure. The scoured structure has a lower stiffness at the 60m point, which subsequently alters the excitation provided to the vehicle by the bridge at this point and along the spans either side of this pier. This variation in the excitation manifests itself as a change in the forced vehicle response due to the vehicle-bridge interaction. Once the vehicle passes the 80m point, the difference between the unscoured and scoured structural responses are less noticeable, so the differences in wavelet coefficients of the vehicle response at these locations are minimised. Fig. 7 shows the difference in apparent profile between the healthy and scoured cases for the same vehicle run of Figs. 5 and 6. At around the scoured location of 60 m, the apparent profile shows the greatest change, which also extends into the spans either side of the scoured pier (between 40m and 80m) as a result of the changed support condition due to scour.

It is worth noting that the Mexican Hat wavelet also allowed scour to be detected when applied to the accelerations in Fig. 6. Subtracting the coefficients is not an issue in this case as the acceleration signals are in phase. This is because the vehicles that cross the bridge have the same speeds and properties.

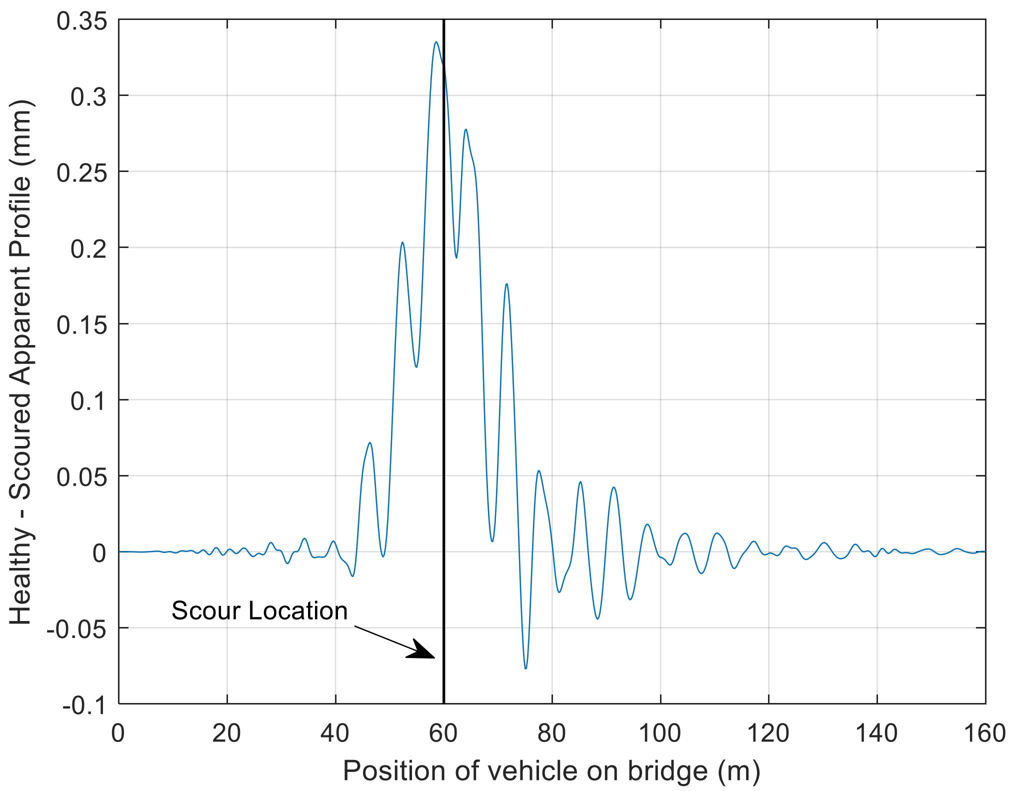

Fig. 7: Difference between healthy and scoured apparent profiles (note: upwards direction taken as positive)

4. Scour Detection using Batches of Runs

The analysis conducted so far has used identical vehicle properties for the healthy and scoured cases. In reality, variations in speed (due to driver behaviour) and carriage mass (fuel, number of passengers etc.) exist between each run. In this section the method is applied to batches of runs, and the effect of vehicle parameter variation (speed and mass) is investigated. Noise is also added to the acceleration signals, and different damage (scour) severities are investigated.

4.1 Properties of fleet

To examine the effects of vehicle mass and speed variations, a population of representative vehicles is created. Normal distributions of carriage mass and velocity are assumed, with mean values of m_c=18.4 tonnes and speed=80 km/h, and standard deviations of ±10% in each case. Fig. 8 shows histograms for the population of carriage body mass and speed used. For each run, these properties are selected with probability in proportion to the frequencies shown. Values of bogie mass, and suspension parameters are maintained constant at the values given in Table 1. The postulated scour detection approach is envisaged to work using acceleration data from the same instrumented train (on a given line), so the only aspects that are expected to vary between runs are vehicle speed (due to driver variation) and carriage mass (due to passenger load etc.). Batches of 200 vehicle runs are generated for each analysis.

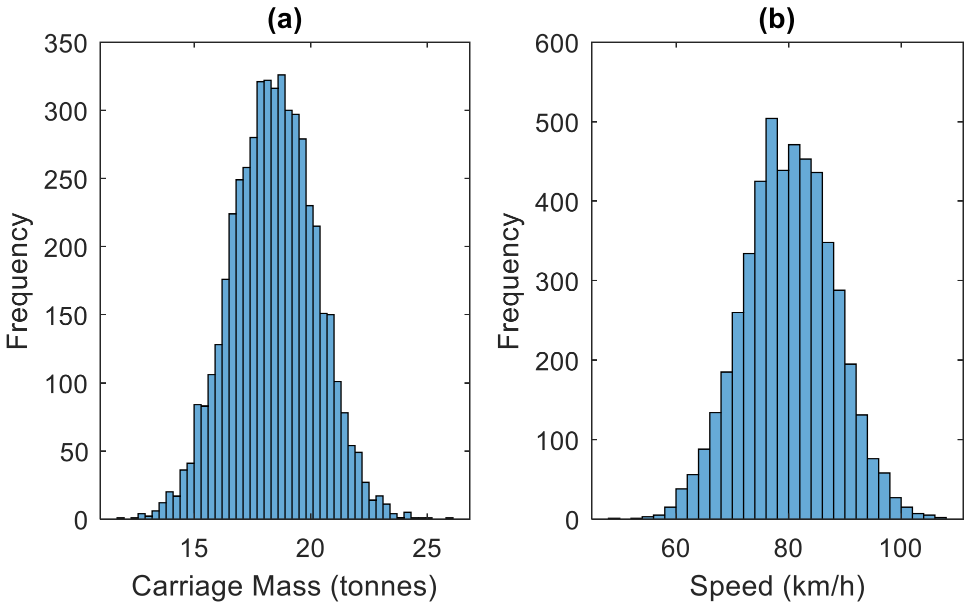

Fig. 8: Histogram of quarter-car fleet properties – (a) carriage mass, (b) speed

4.2 Scour indicator

Three scour scenarios are investigated, namely reductions in foundation stiffness from the healthy case of 30%, 20% and 10% for the pier at the 60 m point of the bridge. For each scenario, a batch of 200 vehicles is simulated crossing the bridge. Noise levels of 5% are added to each acceleration signal according to Eq. (7).

For each run, the CWT, using the Complex Morlet wavelet, is applied to the acceleration signal, and the moduli of the coefficients are calculated. The moduli are then interpolated to the vehicle position on the bridge using a vector *P*. The average of the moduli with respect to position on the bridge is then calculated for the 200 runs. The scour indicator is calculated by subtracting the average moduli for the batch under investigation from the average moduli for the baseline (healthy bridge) batch. A frequency range is selected on which to base a scour indicator. In this case, information from all frequencies in the range from 0.5 Hz to 15 Hz is used. This facilitates automation of the scour detection process and avoids the need for an expert user. It also allows for a universal approach for bridges with different dynamic properties if the same train is used to detect scour on a number of bridges on the line. In mathematical form, the average of the moduli of the coefficients for a batch of vehicles yields a matrix, *M*, with entries corresponding to frequency (i.e. scale) and bridge location, which can be defined as:

$$[M] = \frac{1}{V}\sum_{i=1}^{V}[R_i] \tag{9}$$

where *R* is a matrix of coefficient moduli for each run, interpolated to position on bridge, and *V* is the number of runs in a batch. The scour indicator is defined as the absolute difference between healthy and scoured matrices:

$$[C] = abs([M_{healthy}] - [M_{scour}]) \tag{10}$$

The matrix *C* is summed over all N_s scales in the specified frequency range (0.1 Hz to 15 Hz) in increments of 0.1 Hz (giving N_s=146). This sum at each location is:

$$\{S_j\} = \sum_{i=1}^{N_s}[C_{ij}] \tag{11}$$

for $j \in \{1{:}L\}$ where, *L* is the length of the bridge position vector *P*.

4.3 Analysis and results using preliminary model

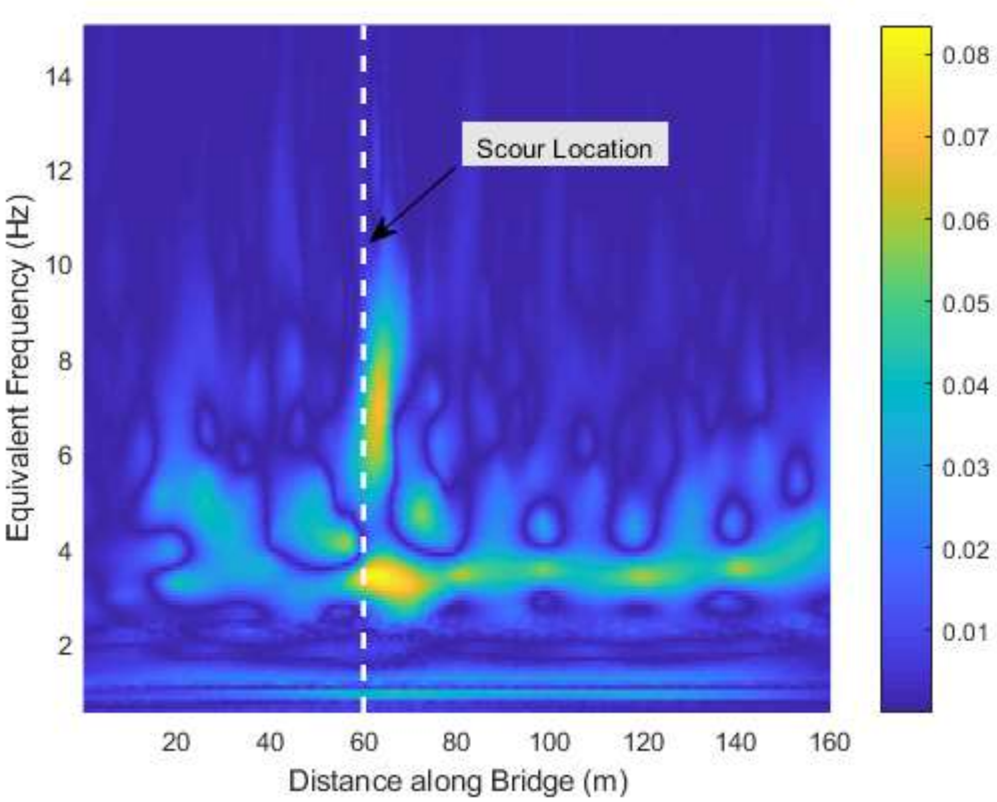

Fig. 9: Matrix *C* for scour of 30% at 60 m point on bridge

Fig. 9 shows the Matrix *C* (Eq. 10) for an example with a 30% reduction in foundation stiffness at the 60 m point on the bridge. It is clear that the largest differences occur at a few different frequencies (shown by the light colours in the plot), and these differences can be combined to form one scour indicator. For each point on the bridge, the sum of the values over every scale can then be taken from the vector *S*, defined in Eq. (11). Fig. 10 plots this vector *S* against location for different severities of scour at the 60 m point and the 120 m point. The differences between two healthy batches is also plotted to show the natural variability in a healthy bridge. It is seen that the maximum value of the vector *S* occurs at approximately the location where scour occurs, and therefore is a reasonable indicator of scour. This maximum value also increases with an increase in damage severity.

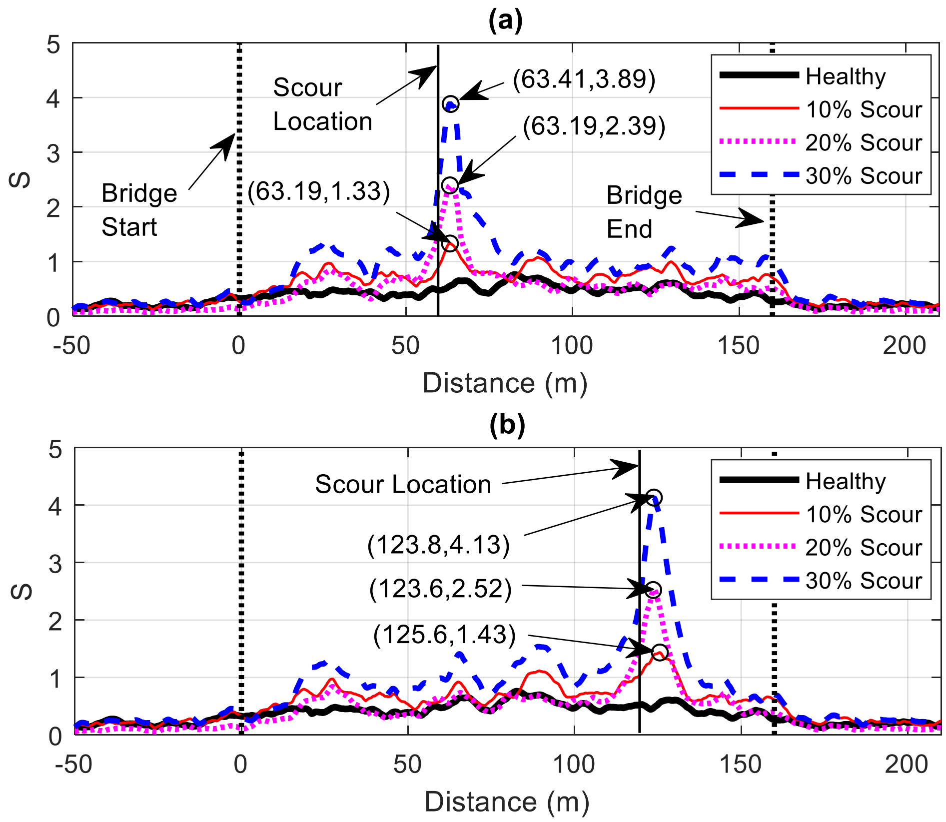

Fig. 10: Vector *S* plotted against bridge position – (a) scour at 60 m, (b) scour at 120 m

5. Analysis using advanced train-track-bridge model and blind simulation tests

In this section, the scour detection method is tested using blind simulation tests, whereby signals are generated using a numerical model by an external party. The external party only provides the vehicle accelerations to the user and the approach is implemented to ascertain if scour can be detected, when the user does not know if/where scour is implemented on a bridge. This is analogous to a real situation, whereby a bridge manager would obtain signals without any knowledge of whether scour exists or not. Additionally, the external party utilises a more advanced numerical model to generate the response signals.

5.1 Model description

In this blind test, the external party was the Norwegian University of Science and Technology (NTNU). They used a two-dimensional model of a train carriage to calculate accelerations from the bogie bounce DOF of the leading bogie for the University College Dublin (UCD) team. A railway track was also included on the bridge.

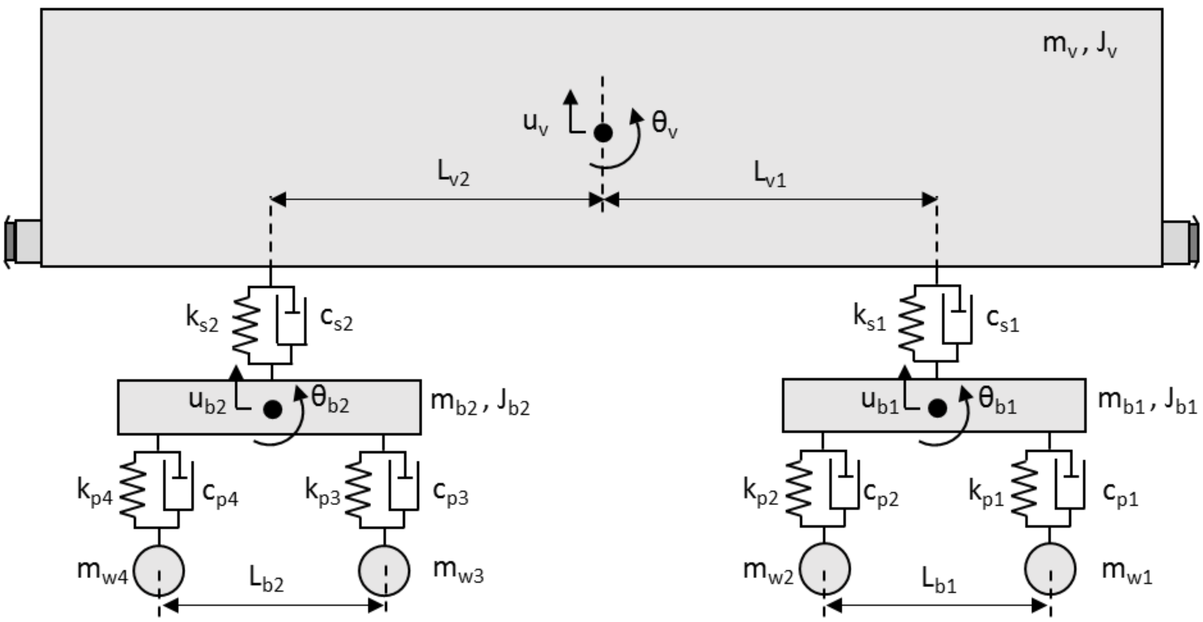

Fig. 11: Advanced vehicle model *A*

Fig. 11 shows a schematic of the 2D vehicle model used by NTNU. A brief description of the model is provided herein with a more detailed explanation available in [39]. There are 10 DOFs in the model; four wheelsets (each of which have one vertical DOF), two bogies (each of which has one vertical and one rotational DOF), and a carriage (that has one vertical and one rotational DOF). The bogies are modelled as rigid bars of mass m_b and moment of inertia J_b while the carriage body is also modelled as a rigid bar having a mass and a moment of inertia denoted as m_v and J_v respectively. The wheelsets are connected to the bogie through a primary suspension system comprising springs with stiffness, k_p, and dampers, c_p, which are connected in parallel. A spring and damper, k_s and c_s, representing the secondary suspension also connects each bogie to the carriage. Small rotations in the model are assumed, which allows for a linearised system of equations of motion to be adopted [50]. The vehicle model described here has been used in other studies [51-53]. The model properties are taken from Iwnick [54] and are listed in Table 3.

Table 3: Vehicle properties [54]

Property	**Symbol**	**Unit**	**Value**
Carriage body mass	m_v	kg	32×10^3
Carriage body moment of inertia	J_v	kg m^2	1.97×10^6
Bogie mass	m_b	kg	2,615
Bogie moment of inertia	J_b	kg m^2	1,476
Wheelset mass	m_{w1} , m_{w2} , m_{w3} , m_{w4}	kg	1,813

Primary suspension stiffness	k_p	N/m	2.40×10^6
Secondary suspension stiffness	k_s	N/m	0.86×10^6
Primary suspension damping	c_p	kN s/m	7
Secondary suspension damping	c_s	kN s/m	16
Distance between axles	L_{b1} , L_{b2}	m	2.56
Horizontal distance between centre of mass of main body and bogie	L_{v1} , L_{v2}	m	9.50

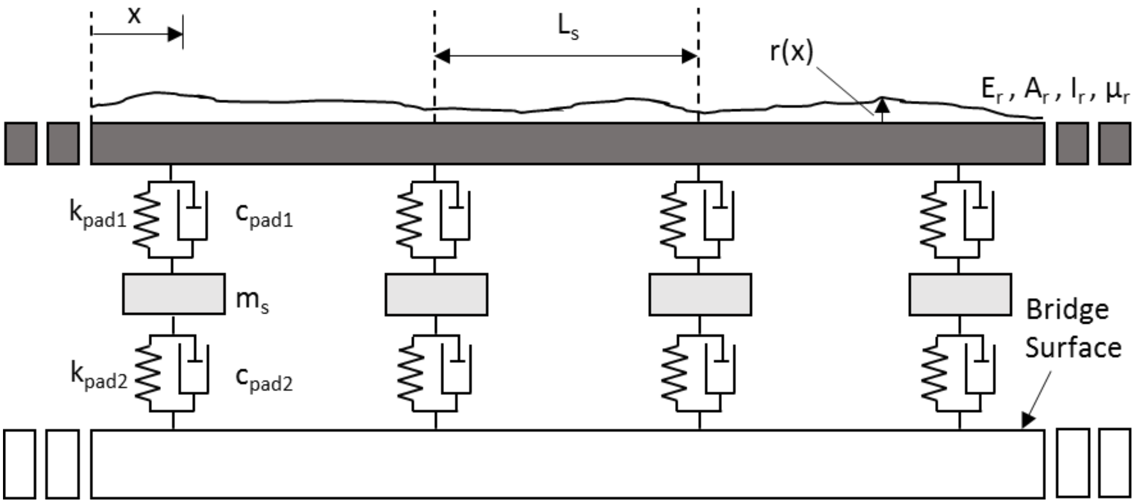

Fig. 12: Track model

The NTNU bridge model includes a track, which lies on top of the bridge (Fig. 12). The track is modelled as a beam supported on a two-layer sprung mass system representing a pad, sleeper and second pad. A surface profile is also included on the track as undertaken previously. Similar track models can be found in the literature [50, 55-57]. The track supports are a distance L_s apart, which represents the sleeper spacing. The track is made of beam elements that have two DOFs at each node. Values of track parameters used in this study are taken from [56]. The complete list of parameters from the model depicted in Fig 12 are shown in Table 4.

Table 4: Track properties [56]

Property	**Symbol**	**Unit**	**Value**
Rail Young's modulus	E_r	N/m^2	2.059×10^{11}
Rail cross-sectional area	A_r	m^2	15.400×10^{-3}
Rail second moment of area	I_r	m^4	6.434×10^{-5}
Rail mass per unit length	μ_r	kg/m	121.280
Pad (above sleeper) stiffness	k_{pad1}	N/m	6.500×10^7
Pad (above sleeper) damping	c_{pad1}	N s/m	7.500×10^4
Mass of sleeper	m_s	kg	251
Sleeper spacing	L_s	m	0.600

Subgrade stiffness	k_{sg}	N/m	77.500 × 10^6
Subgrade damping	c_{sg}	N s/m	3.115 × 10^4
Pad (below sleeper) stiffness	k_{pad2}	N/m	120 × 10^6
Pad (below sleeper) damping	c_{pad2}	N s/m	60 × 10^4

Finally, the train, track and bridge models are coupled in a similar manner to that described in Section 2. The bridge contains the same properties as described in Section 2, except that, in the present application, only six spans are modelled to reduce computational time.

5.2 Blind test

5.2.1 Test Description

In this section a blind test is carried out whereby signals from a scoured bridge crossing are analysed by a user (UCD) who does not know the scour condition a-priori. The signals are generated by an external party (NTNU) using the advanced model described in Section 5.1. Specifically, the NTNU train-track-bridge model is used to generate simulated bogie bounce acceleration measurements from the leading bogie (i.e. DOF u_{b1}). The carriage body mass (m_v), body moment of inertia (J_v) and vehicle speed are randomly selected from a truncated normally distributed population with set mean and standard deviation values. Table 5 presents the population details of these three parameters. The other vehicle parameters remain constant at the values listed in Table 3.

Table 5: Vehicle population details

Property	**Symbol**	**Mean**	**Standard Deviation**	**Minimum**	**Maximum**	**Unit**
Body mass	m_v	32 × 10^3	3.200 × 10^3	16 × 10^3	48 × 10^3	kg
Body moment of inertia	J_v	1.970 × 10^6	0.591 × 10^6	0.985 × 10^6	2.955 × 10^6	kg m^2
Speed	v	105	3.900	50	120	km/h

For each run, NTNU randomly picks the three vehicle properties from the population described in Table 5. Each run is described herein as an event (i.e. Event 1, Event 2 etc.). 5% noise is also added using the method described in Eq. (7). In total, 1755 events were sent to UCD and labelled in consecutive order. At some point in time (unknown to UCD), scour is introduced through a reduction in spring stiffness k_f at an unknown location on the bridge. Therefore, every event occurring before this event comprises a healthy bridge and every event after this has one scoured pier. At the time of analysing the accelerations, the severity and event number when the scour happens, is unknown. In addition, there is an unknown approach and exit length over which the vehicle travels before and after the bridge. Therefore, the bridge start and end points must be estimated (in keeping with a real situation). It is known that the first 200 events of the test are for a healthy bridge case. These runs are therefore available to establish a baseline healthy bridge response.

5.2.2 Scour Detection Procedure

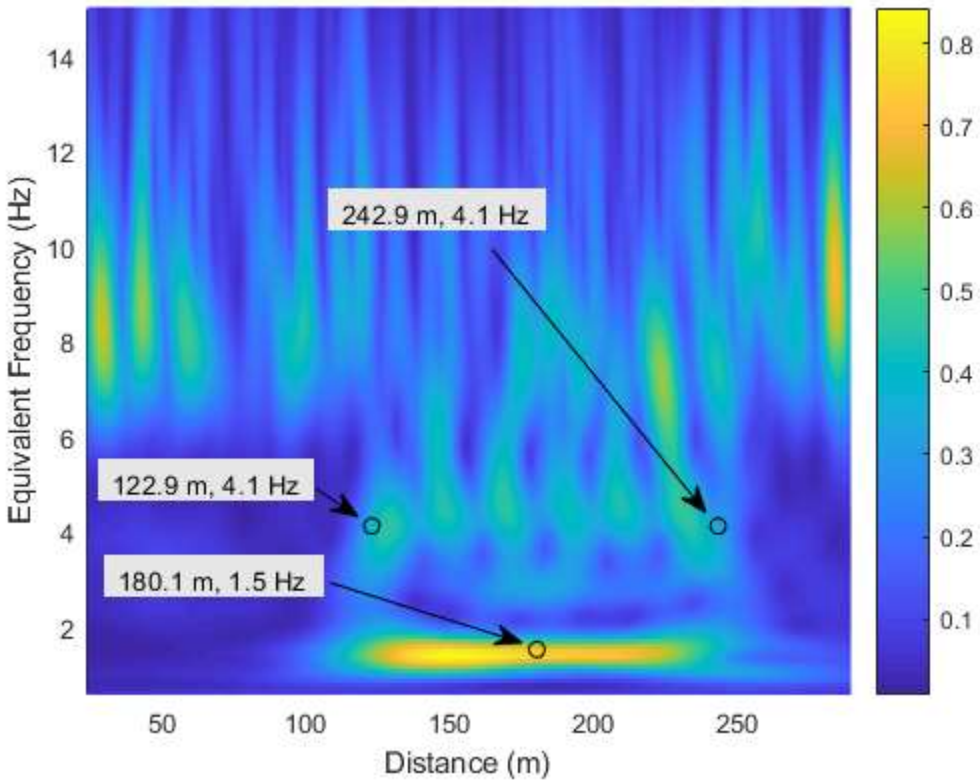

Fig. 13: Estimation of bridge start and end using average coefficient moduli of 200 runs

The first step in the analysis is to calculate the average matrix for the first 200 healthy events, taken as the baseline, i.e. the matrix *M*, described in Eq. (9). Fig. 13 plots this matrix and it is clear that there are frequencies that have an amplitude in a certain region, which are due to the bridge. For example, frequencies at approximately 4.1 Hz and 1.5 Hz relate to the bridge and, from this plot, the bridge start and end can be estimated to be at 122.9 m and 242.9 m respectively. This is reasonable as we know the bridge to be 120 m in length. The 4.1 Hz peaks may be attributed to a frequency of the bridge system. In the bridge model, described in Section 2, the first eight frequencies of the system ranged between 3.69 Hz and 4.33 Hz and the 4.1 Hz value observed in Fig. 13 falls within this range. However, this information does not actually need to be known beforehand, and Fig. 13 clearly shows this without any need for prior information. Another dominant frequency when the vehicles are on the bridge is at 1.5 Hz. This is related to the speed of the vehicle and the span length. The mean speed of the population is 105 km/h (29.167 m/s). For a span length of 20 m, the span crossing frequency is 1.46 Hz (i.e. 29.167/20). Again, this frequency is evident in the figure and does not need to be calculated.

Once the bridge ends are identified, the next step is to create batches of vehicles to input to the scour identification process. Batches of 20, 50, 100 and 200 vehicle crossings are each tested in order to ascertain how the method works with different numbers of vehicles per batch. The batches overlap akin to a moving average. For example, if 200 is the number of vehicles in the batch, the first batch consists of events 1 to 200, the second 2 to 201 and so on. It is shown in the previous section that the maximum value and location of the vector S (defined in Eq. (11)) is a strong metric for detecting the presence of scour. This maximum value is defined here as the Scour Indicator (abbreviated S.I.).

5.2.3 Results

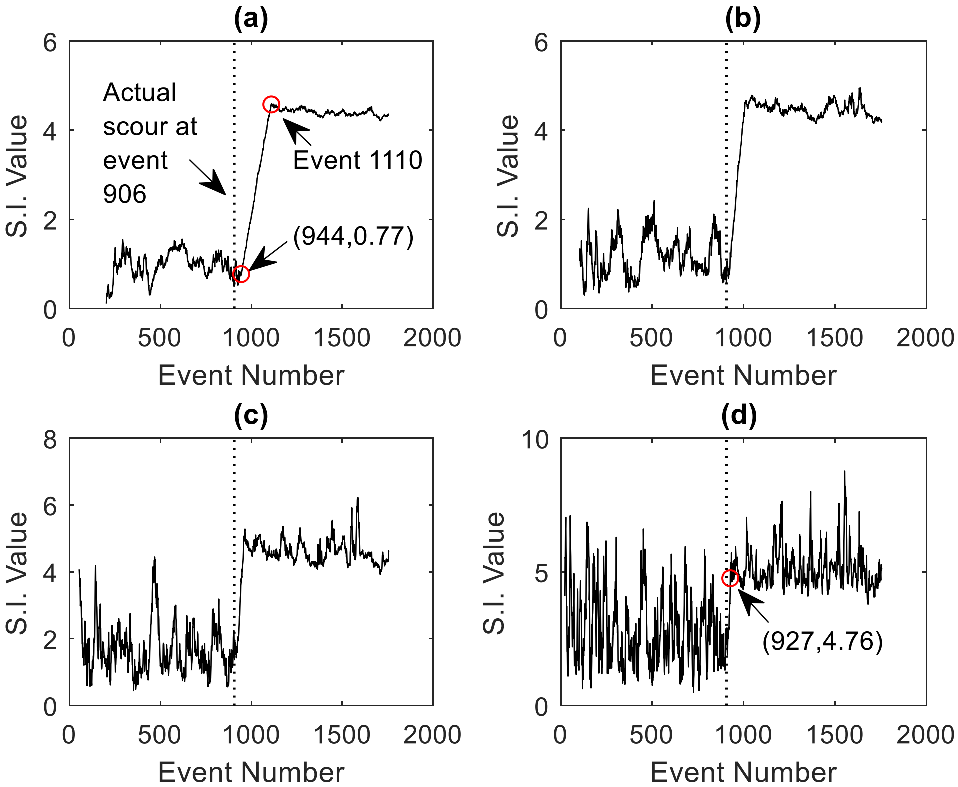

Fig. 14: S.I. vs event number – (a) batches of 200 vehicles, (b) batches of 100 vehicles, (c) batches of 50 vehicles, (d) batches of 20 vehicles

Fig. 14 shows the value of S.I. for batches containing different numbers of vehicles. Here, each batch is labelled with the event number of the last vehicle in the batch. For example, the 944 point marked in Fig. 14(a) is the batch of vehicles containing events 745 to 944, and the 927 point marked in Fig. 14(d) is the batch containing events 908 to 927. The actual event number and severity of scour is in fact Event 906 with a scour severity of 30% implemented at the 40 m point on the bridge. Fig. 14 shows that the method is quite effective at detecting the scour anomaly. It is seen in Fig. 14(a) that at around Event 944, S.I. begins to increase. The actual scour is at event 906 but the batch 745 to 944 comprises vehicle runs from both the bridge in a healthy and scoured state. As a result, subsequent batches contain a higher ratio of scoured to healthy runs meaning that the S.I. continues to rise after this point. At Event 1110, the S.I. starts to level off. At this point the events in the batch are from 910 to 1100, so all events are scoured events. However, the scour can be detected long before the S.I. reaches a peak. The first clear sign of scour is when the S.I starts to increase irregularly, which is approximately at Event 944 here.

Fig. 14 shows that lower numbers of batches can also be used. For the lowest number of vehicles in a batch - Fig. 14(d) (20 vehicle crossings), it can be seen that S.I. has much more variability but it is still possible to detect scour, as the jump discontinuity is still evident. However, using a lower number per batch increases the amount of false-positive indications of scour, which is a trade-off in an effort to detect scour earlier.

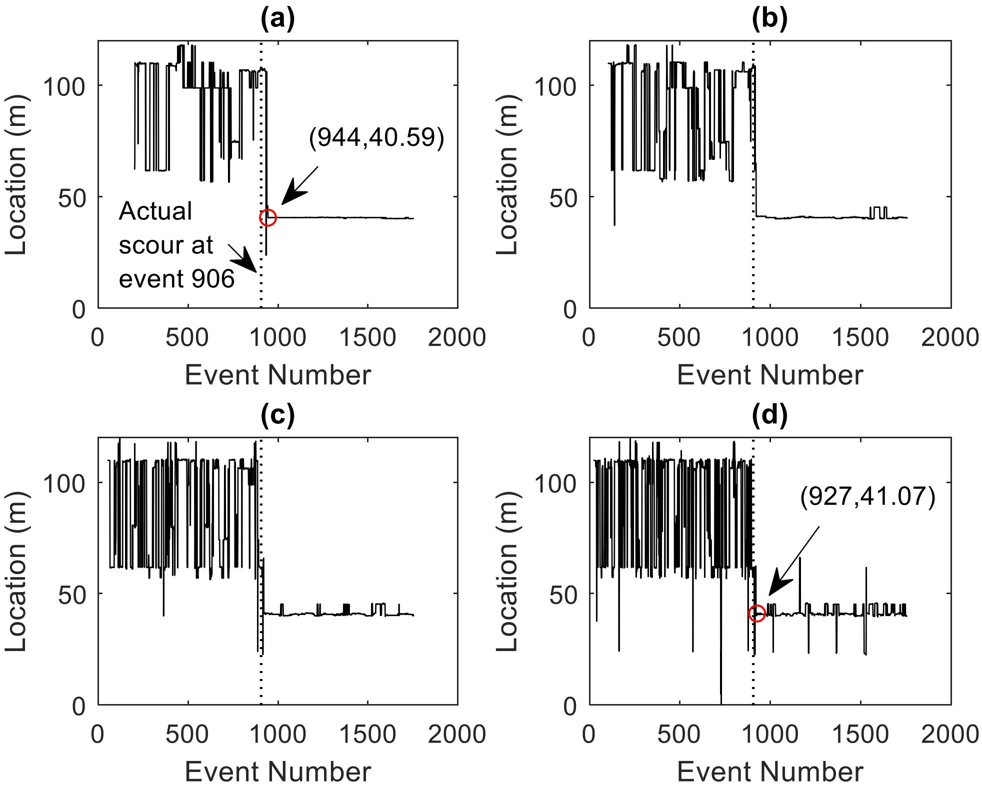

Fig. 15: Scour Indicator maximum location point – (a) batches of 200 vehicles, (b) batches of 100 vehicles, (c) batches of 50 vehicles, (d) batches of 20 vehicles

Fig. 15 demonstrates that the S.I. can also indicate the location on the bridge at which the maximum S.I is obtained, i.e. the location of the scoured pier. Fig. 15 shows the position on the bridge corresponding to the maximum value of the scour indicator. Before the scour location (i.e. Event 944), the location of the maximum S.I. fluctuates significantly. However, after this event, the location is somewhat constant at around the 40 m position on the bridge. This is in fact the location of the scoured pier. Similar results can be derived from the remaining plots with lower numbers per batch. The location feature of the S.I. could very well be used on its own, as it is seen in Fig. 15 that the location of scour is being isolated quite well.

5.3 Effect of varying scour location and severity

This section tests how the S.I. behaves for different locations and severity of scour. It is worth noting that this part of the analysis was not blind like the previous section. Here, the location and severity of scour was provided. There are five piers supported by deformable springs in this study (at 20 m, 40 m, 60 m, 80 m and 100 m point) and scour severities (stiffness reduction) of 7.5%, 15%, 22.5% and 30% for each location. This makes a total of 20 scour scenarios investigated. For each case, a batch of 200 runs (all over the scoured bridge) is compared with a batch of 200 healthy runs. Fig. 16 and Table 6 show the S.I. value and pier location predictions for each scour scenario.

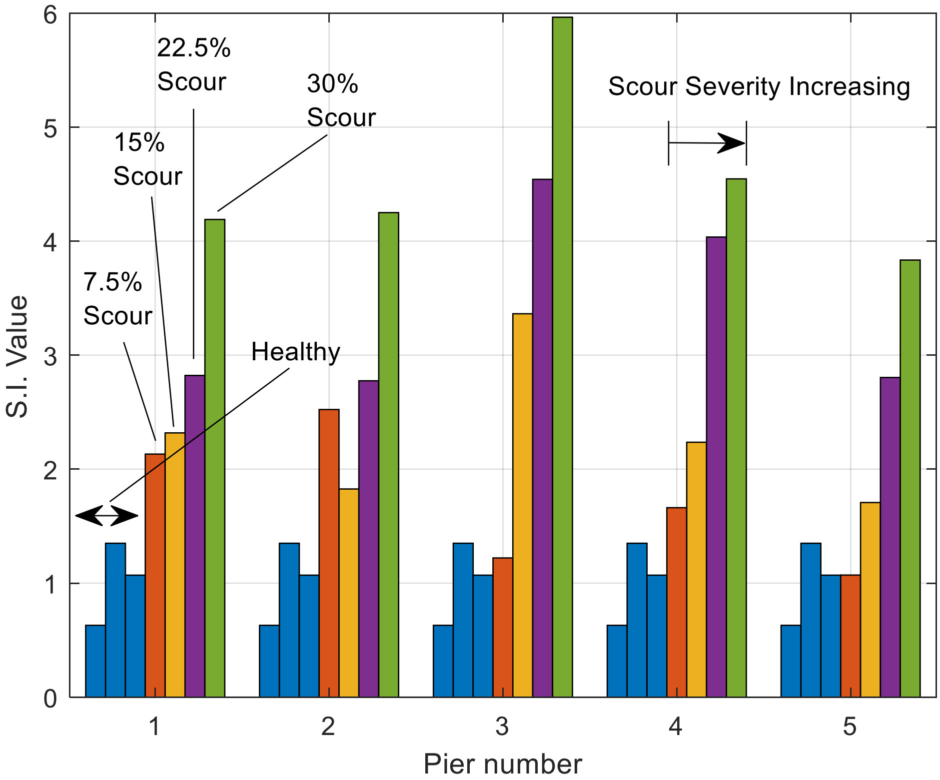

Fig. 16: Scour Indicator value for different scour severities at each pier location (where Pier 1 is at 20 m)

Table 6: Maximum Scour Indicator locations with false estimations highlighted

		Actual Scour Locations				
		20 m	**40 m**	**60 m**	**80 m**	**100 m**
Scour Severities	**7.5%**	106.1 m	109.9 m	62.4 m	106.7 m	102.6 m
	15.0%	22.8 m	45.5 m	64.8 m	81.8 m	99.8 m
	22.5%	21.4 m	40.5 m	63.0 m	81.0 m	104.8 m
	30.0%	22.0 m	40.2 m	62.6 m	82.0 m	104.4 m

Fig. 16 shows how the value of the S.I. changes with different locations and severities of scour. The same scour severities are investigated for each scour location. Also shown is the S.I. value obtained for three healthy cases. It is seen from the figure that the S.I. generally increases with scour severity which corroborates the findings of the simpler model. However, the indicator does not always provide consistent results. For example, Pier 2 has a greater S.I. value for the 7.5% scour case than the 15% scour case, and one of the healthy cases in Pier 3 has a higher S.I. value than for the 7.5% scour case. As well as this, each of the three healthy cases have slightly different S.I. values. These discrepancies are unrelated to scour and are as a result of the natural variability in the vehicle batches. Also of note is that the value of the S.I. is generally larger for the scour locations closer to the centre pier (at the 60 m point mark). This is expected from examining the healthy mode shape depicted in Fig. 3, which shows that the bridge experiences higher modal amplitudes closer to the centre of the bridge. As this S.I. uses the difference between healthy and scoured cases, it means that the value of S.I. will be slightly higher for scour locations closer to the centre of the bridge. However, broadly speaking the value of S.I. at a scoured location will be higher than the equivalent healthy case. Finally, Table 6 shows the location of the maximum S.I. value and the actual location of scour. It is seen that for scour severities of 7.5 %, the indicated location is false for three cases. Clearly, for this scour level, the maximum value is too close to that of a healthy bridge case and the location corresponds to an arbitrary point on the bridge unrelated to scour. For these reasons, it may be deduced that the method may not perform very well for low scour levels. Nevertheless, aside from the three incorrect scour estimations shown, all other scenarios have predicted the correct locations with errors ranging from between 0.2 m and 5.5 m, which is sufficiently close to the affected piers.

5.4 Practical considerations for real applications

The approach demonstrated numerically in this paper may be useful to detect and monitor the presence of scour erosion in railway bridges. The method is predicated on the concept that scour induces a loss in foundation stiffness, resulting from geometrical and soil strain-related considerations. The approach is unsuited to quantifying the magnitude of scour affecting a given foundation directly, as the relationship between scour depth and resulting stiffness loss relies on several interrelated parameters. Instead, it is envisaged that the scour-related stiffness loss may be monitored by analysis of the signals measured by numerous train passages, and this information may be used to trigger visual inspections and associated remediation works by infrastructure managers.

In terms of the S.I. threshold that could be used at a decision-making level to prioritise an inspection, there are several methodologies available to support decision making. One such approach relies on correlating a S.I. value to a measured scour condition, obtained from diving records (or installed scour-depth measuring instrumentation) at discrete times. Based on existing scour rating approaches adopted by railway authorities, a limiting S.I. value can be specified based on the value measured for a critical scour magnitude affecting the structure. While simple, this approach is disadvantageous as it relies on additional scour depth information being measured and will be prone to errors due to the nonlinear relationship between the scour condition and resulting stiffness reduction, and subsequent S.I. readings (as mentioned previously).

A more viable approach is to use statistical techniques to monitor the natural repeatability in measurements in the healthy (unscoured) condition, which will vary from site to site and also due to driver behaviour. When subsequent changes to the healthy (benchmark) condition are identified, sample statistics will plot outside of the normal operating control limits. A trigger could be based on deviations in these measurements exceeding the mean plus a portion of the standard deviation. One such approach used previously for damage detection is control charts [58]. This type of approach would not require additional scour depth information, and is ideal for automatic monitoring. Therefore, this may be a useful approach for scour monitoring using the S.I. value postulated in this paper.

6. Conclusions

This paper has numerically investigated the feasibility of detecting bridge scour using accelerations measured on the bogie of a passing train carriage. A scour indicator, defined as the difference in average CWT coefficients between healthy and scoured batches of train crossings is shown to be quite effective at not only detecting the presence of scour but in also locating it. The approach described here is novel in the context of scour detection and is advantageous in that it has been shown to work under normal train operational speeds. This indicates that a bridge can be monitored for scour under usual service conditions and does not require specialist monitoring vehicles. Although no field tests have been carried out, the scour indicator has performed quite well in both numerical models that were tested, which included added measurement errors and train-bridge interaction effects. The results will be of interest to the ongoing development of the vibration-based scour monitoring field.

Acknowledgements

The authors wish to acknowledge the financial support received from Science Foundation Ireland under the US-Ireland Research Partnership Scheme.

References

[1] L. Hamill, Bridge Hydraulics, E.& F.N. Spon, Routledge, London & New York, 1999.

[2] B. Maddison, Scour failure of bridges, Proceedings of the Institution of Civil Engineers-Forensic Engineering 165(1) (2012) 39-52.

[3] K. Wardhana, F.C. Hadipriono, Analysis of recent bridge failures in the United States, Journal of Performance of Constructed Facilities 17(3) (2003) 144-150.

[4] F. Federico, G. Silvagni, F. Volpi, Scour vulnerability of river bridge piers, Journal of geotechnical and geoenvironmental engineering 129(10) (2003) 890-899.

[5] M. Forde, D. McCann, M. Clark, K. Broughton, P. Fenning, A. Brown, Radar measurement of bridge scour, NDT & E International 32(8) (1999) 481-492.

[6] J.L. Briaud, F.C. Ting, H. Chen, R. Gudavalli, S. Perugu, G. Wei, SRICOS: Prediction of scour rate in cohesive soils at bridge piers, Journal of Geotechnical and Geoenvironmental Engineering 125(4) (1999) 237-246.

[7] L.J. Prendergast, M.P. Limongelli, N. Ademovic, A. Anzlin, K. Gavin, M.A. Zanini, Structural Health Monitoring for Performance Assessment of Bridges under Flooding and Seismic Actions, Structural Engineering International 28(3) (2018) 296-307.

[8] D. Hughes, G.E. Ramey, M.L. Hughes, Effects of extreme scour and soil subgrade modulus on bridge pile bent buckling, Practice Periodical on Structural Design and Construction 12(2) (2007) 96-108.

[9] L.J. Prendergast, K. Gavin, A review of bridge scour monitoring techniques, Journal of Rock Mechanics and Geotechnical Engineering 6(2) (2014) 138-149.

[10] T. Bao, R.A. Swartz, S. Vitton, Y. Sun, C. Zhang, Z. Liu, Critical insights for advanced bridge scour detection using the natural frequency, Journal of Sound and Vibration 386 (2017) 116-133.

[11] J.L. Briaud, S. Hurlebaus, K.A. Chang, C. Yao, H. Sharma, O.Y. Yu, C. Darby, B.E. Hunt, G.R. Price, Realtime monitoring of bridge scour using remote monitoring technology, Texas A&M University System, Texas, 2011.

[12] A. Elsaid, R. Seracino, Rapid assessment of foundation scour using the dynamic features of bridge superstructure, Construction and Building Materials 50 (2014) 42-49.

[13] J.V. Klinga, A. Alipour, Assessment of structural integrity of bridges under extreme scour conditions, Engineering Structures 82 (2015) 55-71.

[14] S. Ju, Determination of scoured bridge natural frequencies with soil–structure interaction, Soil Dynamics and Earthquake Engineering 55 (2013) 247-254.

[15] L.J. Prendergast, K. Gavin, D. Hester, Isolating the location of scour-induced stiffness loss in bridges using local modal behaviour, Journal of Civil Structural Health Monitoring 7(4) (2017) 483-503.

[16] L.J. Prendergast, D. Hester, K. Gavin, Determining the presence of scour around bridge foundations using vehicle-induced vibrations, Journal of Bridge Engineering 21(10) (2016) Article ID 04016065.

[17] S. Foti, D. Sabia, Influence of foundation scour on the dynamic response of an existing bridge, Journal of Bridge Engineering 16(2) (2010) 295-304.

[18] C.-C. Chen, W.-H. Wu, F. Shih, S.-W. Wang, Scour evaluation for foundation of a cable-stayed bridge based on ambient vibration measurements of superstructure, NDT & E International 66 (2014) 16-27.

[19] W. Xiong, B. Kong, P. Tang, J. Ye, Vibration-Based Identification for the Presence of Scouring of Cable-Stayed Bridges, Journal of Aerospace Engineering 31(2) (2018) 04018007.

[20] X. Kong, C.S. Cai, B. Kong, Damage detection based on transmissibility of a vehicle and bridge coupled system, Journal of Engineering Mechanics 141(1) (2014) Article ID 04014102.

[21] A. Malekjafarian, P.J. McGetrick, E.J. OBrien, A review of indirect bridge monitoring using passing vehicles, Shock and vibration 2015 (2015) Article ID 286139.

[22] D. Hester, A. González, A discussion on the merits and limitations of using drive-by monitoring to detect localised damage in a bridge, Mechanical Systems and Signal Processing 90 (2017) 234-253.

[23] Y. Yang, J.P. Yang, State-of-the-art review on modal identification and damage detection of bridges by moving test vehicles, International Journal of Structural Stability and Dynamics 18(02) (2018) Article ID 1850025.

[24] X. Zhu, S.-S. Law, Structural health monitoring based on vehicle-bridge interaction: Accomplishments and challenges, Advances in Structural Engineering 18(12) (2015) 1999-2015.

[25] Y.B. Yang, C.W. Lin, J.D. Yau, Extracting bridge frequencies from the dynamic response of a passing vehicle, Journal of Sound and Vibration 272(3-5) (2004) 471-493.

[26] C. Lin, Y. Yang, Use of a passing vehicle to scan the fundamental bridge frequencies: An experimental verification, Engineering Structures 27(13) (2005) 1865-1878.

[27] Y. Oshima, T. Yamaguchi, Y. Kobayashi, K. Sugiura, Eigenfrequency estimation for bridges using the response of a passing vehicle with excitation system, Proceedings of the fourth international conference on bridge maintenance, safety and management, Seoul, Korea, 2008, pp. 3030-3037.

[28] Y.W. Kwon, H. Bang, The finite element method using MATLAB, CRC press, Boca Raton, Florida, 2000.

[29] R.W. Clough, J. Penzien, Dynamics of Structures, McGraw-Hill1993.

[30] E.J. OBrien, P. McGetrick, A. González, A drive-by inspection system via moving force identification, Smart Structures and Systems 13(5) (2014) 821-848.

[31] P.J. McGetrick, C.W. Kim, A. González, E.J. Brien, Experimental validation of a drive-by stiffness identification method for bridge monitoring, Structural Health Monitoring 14(4) (2015) 317-331.

[32] T. Ogden, Essential wavelets for statistical applications and data analysis, Springer Science & Business Media, New York, 2012.

[33] G. Strang, T. Nguyen, Wavelets and filter banks, Wellesley-Cambridge Press, Wellesley, MA 02181, 1996.

[34] P.J. McGetrick, C.W. Kim, A parametric study of a drive by bridge inspection system based on the Morlet wavelet, Key Engineering Materials 569 (2013) 262-269.

[35] A. Khorram, F. Bakhtiari-Nejad, M. Rezaeian, Comparison studies between two wavelet based crack detection methods of a beam subjected to a moving load, International Journal of Engineering Science 51 (2012) 204-215.

[36] E.J. OBrien, P. Quirke, C. Bowe, D. Cantero, Determination of railway track longitudinal profile using measured inertial response of an in-service railway vehicle, Structural Health Monitoring (2017) 1475921717744479.

[37] L.J. Prendergast, K. Gavin, A comparison of initial stiffness formulations for small-strain soil–pile dynamic Winkler modelling, Soil Dynamics and Earthquake Engineering 81 (2016) 27-41.

[38] BSS Council. Prestandard and commentary for the seismic rehabilitation of buildings - Report FEMA-356, Washington, DC, 2000.

[39] D. Cantero, T. Arvidsson, E. OBrien, R. Karoumi, Train–track–bridge modelling and review of parameters, Structure and Infrastructure Engineering 12(9) (2016) 1051-1064.
[40] S. Oztoprak, M. Bolton, Stiffness of sands through a laboratory test database, Géotechnique 63(1) (2013) 54-70.
[41] T. Mei, H. Li, Measurement of vehicle ground speed using bogie-based inertial sensors, Proceedings of the Institution of Mechanical Engineers, Part F: Journal of Rail and Rapid Transit 222(2) (2008) 107-116.
[42] P. Quirke, D. Cantero, E.J. OBrien, C. Bowe, Drive-by detection of railway track stiffness variation using in-service vehicles, Proceedings of the Institution of Mechanical Engineers, Part F: Journal of Rail and Rapid Transit 231(4) (2017) 498-514.
[43] A. Malekjafarian, E.J. OBrien, Identification of bridge mode shapes using short time frequency domain decomposition of the responses measured in a passing vehicle, Engineering Structures 81 (2014) 386-397.
[44] X.Q. Zhu, S.S. Law, Moving loads identification through regularization, Journal of engineering mechanics 128(9) (2002) 989-1000.
[45] E.J. OBrien, P.C. Fitzgerald, A. Malekjafarian, E. Sevillano, Bridge damage detection using vehicle axle-force information, Engineering Structures 153(Supplement C) (2017) 71-80.
[46] M.R. Taha, A. Noureldin, J. Lucero, T. Baca, Wavelet transform for structural health monitoring: a compendium of uses and features, Structural Health Monitoring 5(3) (2006) 267-295.
[47] A. Teolis, J.J. Benedetto, Computational signal processing with wavelets, Birkhäuser, Cham, Switzerland, 1998.
[48] M.R. Taha, A. Noureldin, A. Osman, N. El-Sheimy, Introduction to the use of wavelet multiresolution analysis for intelligent structural health monitoring, Canadian Journal of Civil Engineering 31(5) (2004) 719-731.
[49] P. Quirke, C. Bowe, E.J. OBrien, D. Cantero, P. Antolin, J.M. Goicolea, Railway bridge damage detection using vehicle-based inertial measurements and apparent profile, Engineering Structures 153 (2017) 421-442.
[50] K. Nguyen, J. Goicolea, F. Galbadon, Comparison of dynamic effects of high-speed traffic load on ballasted track using a simplified two-dimensional and full three-dimensional model, Proceedings of the Institution of Mechanical Engineers, Part F: Journal of Rail and Rapid Transit 228(2) (2014) 128-142.
[51] P. Lou, Finite element analysis for train–track–bridge interaction system, Archive of Applied Mechanics 77(10) (2007) 707-728.
[52] X. Lei, N.A. Noda, Analyses of dynamic response of vehicle and track coupling system with random irregularity of track vertical profile, Journal of sound and vibration 258(1) (2002) 147-165.
[53] Y.Q. Sun, M. Dhanasekar, A dynamic model for the vertical interaction of the rail track and wagon system, International Journal of Solids and Structures 39(5) (2002) 1337-1359.
[54] S. Iwnick, Manchester benchmarks for rail vehicle simulation, Vehicle System Dynamics 30(3-4) (1998) 295-313.
[55] W. Zhai, Two simple fast integration methods for large-scale dynamic problems in engineering, International journal for numerical methods in engineering 39(24) (1996) 4199-4214.
[56] W. Zhai, K. Wang, J. Lin, Modelling and experiment of railway ballast vibrations, Journal of sound and vibration 270(4-5) (2004) 673-683.
[57] F. Lu, D. Kennedy, F. Williams, J. Lin, Symplectic analysis of vertical random vibration for coupled vehicle–track systems, Journal of Sound and Vibration 317(1-2) (2008) 236-249.

[58] J. Kullaa, Damage detection of the Z24 bridge using control charts, Mechanical Systems and Signal Processing 17(1) (2003) 163-170.